Density-functional theory for ensembles of fractionally occupied states. II. Application to the He atom

L. N. Oliveira,* E. K. U. Gross, and W. Kohn
Department of Physics, University of California, Santa Barbara, California 93106
(Received 21 October 1987)

The two density-functional methods of calculating excitation energies proposed in the preceding paper, combined with the recently formulated quasi-local-density approximation for the equiensemble exchange-correlation energy functional [W. Kohn, Phys. Rev. A **34**, 737 (1986)], are applied to the He atom. Although the splittings between nearly degenerate levels with different angular momenta are badly overestimated, in both approaches the averages over angular momentum and spin of the experimental excitation energies measured from the ionization threshold are reproduced within a few percent. The computed self-consistent ensemble-averaged densities and the Kohn-Sham potentials associated with them are discussed.

I. INTRODUCTION

This paper concludes a three-part series dedicated to fractionally occupied excited states in density-functional theory. The first paper[1] in the series, hereafter referred to as paper I, generalized the Rayleigh-Ritz principle to ensembles of unequally weighted states. On the basis of this development, the second paper,[2] hereafter referred to as paper II, extended Theophilou's equiensemble density-functional formalism[3] to ensembles of fractionally occupied states. Out of that work came two formally exact expressions for the excited-state energies. One of them—Eq. (61) in paper II, an expression implicit in Theophilou's formulation[3]—relates the excitation energies to differences between equiensemble energies; we shall refer to this approach to the calculation of energies as the *equiensemble density* method. The other—Eq. (65) in paper II—relates the excitation energies to differences between Kohn-Sham[4] single-particle eigenvalues; we shall name this alternative approach the *fractional occupation* method, since the self-consistent equations that must be solved involve fractionally occupied orbitals.

In this third paper in the series, we apply both procedures to the He atom, to calculate its excitation spectrum. For this application (as well as for other applications), approximations are necessary to make practical the formal expressions underlying the two approaches. In the equiensemble density method, a suitable approximation is provided by the recently derived[5] expressions for the exchange-correlation energy functional and potential. In the fractional density approach, a necessary additional development will be presented in this paper.

We choose He to try these approximations because of its well-known simply structured spectrum,[6] with negligible spin-orbit splittings. The reduced atomic number offers an additional advantage, since the relatively small nuclear potential adds prominence to exchange and correlation effects. In both approaches, our numerical results for the binding energies (i.e., the energies reckoned from the ionization threshold) averaged over angular momentum and spin lie within a few percent of the similarly averaged experimental binding energies.[6] By contrast, the typical deviation between the angular-momentum-resolved calculated and experimental binding energies is much larger, of the order of 20%; this indicates that our approximate procedures have limited energy resolution, a shortcoming for which our discussion of the calculated spectra proposes an explanation.

A second, less serious limitation of our numerical methods derives from the quasi-local-density approximation[5] for the equiensemble exchange-correlation energy functional, on which both procedures are founded. Reference 5 assumes that, for sufficiently large excitation energies, the equiensemble becomes equivalent to the thermal ensemble. Unfortunately, for a Coulomb potential the partition function diverges at any nonzero temperature, so that no thermal ensemble can be constructed, and the analysis of Ref. 5 is inapplicable. Since the partition function for a confined atom is well defined, we circumvent this difficulty by enclosing the atomic system in a spherical box. For small boxes, one would expect this artificial procedure to distort considerably the atomic energies. By working with large radii, $R \approx 100$ a.u., and monitoring the dependence of the calculated energies on R, we limit such distortions to less than 1% of the computed binding energies. This gives us confidence in our admittedly inelegant expedient.

Besides gauging the accuracy of the density-functional approaches to the calculation of excitation energies, our application is instrumental in comparing them with the transition state approach.[7] Although Slater's method bears formal similarities with the fractional occupation method, the two procedures are not equivalent. One distinction derives from the different approximations for the exchange-correlation potential: while Ref. 7 employs the ground-state exchange potential, the potential in the fractional occupation method derives from the more refined analysis in Ref. 5. However, even if the ground-state exchange potential is substituted for the ensemble potential, the fractional occupation and the transition state ap-

proaches remain different, because they prescribe different occupations for the single-particle levels. To compute the second excitation energy of the He atom, for example, the transition-state formula assigns occupations of $\frac{3}{2}$ to the $1s$ orbital and $\frac{1}{2}$ to the $2p$ orbital; our approach prescribes occupations of $\frac{96}{85}$, to the $1s$ orbital, $\frac{44}{85}$ to the $2s$ orbital, and $\frac{6}{17}$ to the $2p$ orbital. Generally, one method can not be derived from the other, the fractional occupation approach providing an alternative to, and not a refinement of the transition-state prescription. To compare them, we have to examine the accuracy of the results they produce.

On the average, compared with the experimental spectrum, the results of both the fractional occupation and the equiensemble approaches are significantly more accurate than those of the transition-state approach. The latter systematically underestimates the binding energies by $\approx 40\%$. This discrepancy reflects a conceptual inconsistency, the unjustified extrapolation of the ground-state exchange potential to excited states. As one would expect, the errors in the density-functional procedures, deriving from the more appropriate approximation in Ref. 5, are smaller.

This report is divided in four sections. In an attempt to make it self-contained, we recapitulate in Sec. II the most important results of paper II and of Ref. 5. That section also introduces the additional approximation necessary to make operative the fractional density approach and outlines the numerical procedures involved in the equiensemble density, the fractional density and the Slater transition-state approaches. The numerical results are discussed in Sec. III, and Sec. IV summarizes our conclusions. Finally, the Appendix discusses the computation of the energy, entropy, and chemical potential of a homogeneous electron gas at finite temperatures.[8–11] The first two thermodynamical functions enter the quasi-local-density approximation[5] for the exchange-correlation energy functional, while the third defines the exchange-correlation potential.[5]

II. COMPUTATIONAL METHODS

This section describes the two alternative procedures determining excitation energies in density-functional theory and reviews Slater's transition-state approach. We emphasize the practical aspects of the procedures; the basic formulations, detailed in paper II, merit only cursory recapitulation. For clarity, we discuss the three methods separately, first the equiensemble density approach, then the fractional occupation approach, and finally the transition-state approach.

A. The equiensemble density approach

1. Basic equations

The central quantity in the equiensemble formalism[2,3] is the equiensemble density $\rho^M(r)$, defined by

$$\rho^M(r)=\frac{1}{M}\sum_{m=1}^{M}\langle\psi_m\,|\,\hat{\rho}(r)\,|\,\psi_m\rangle\ , \tag{1}$$

where $\hat{\rho}(r)$ denotes the density operator and the $|\psi_m\rangle$ ($1\le m\le M$) are the lowest M eigenstates of the interacting Hamiltonian. The latter is of the form $\hat{H}=\hat{T}+\hat{U}+\hat{V}$, where $\hat{T}$ is the kinetic energy, $\hat{U}$ the Coulomb interaction, and $\hat{V}=\int\hat{\rho}(r)v(r)d^3r$ the external potential. The following self-consistent equations determine $\rho^M(r)$:

$$-\tfrac{1}{2}\nabla^2\varphi_j(r)+v_s[\rho^M](r)\varphi_j(r)=\varepsilon_j\varphi_j(r)\ , \tag{2a}$$

$$v_s[\rho^M](r)=v(r)+\int\frac{\rho^M(r')}{|r-r'|}d^3r'+v_{xc}^M[\rho^M](r)\ , \tag{2b}$$

and

$$\rho^M(r)=\frac{1}{M}\sum_{m=1}^{M}\sum_j f_{mj}\,|\,\varphi_j(r)\,|^2\ . \tag{2c}$$

Here, the $\varphi_j(r)$ and ε_j are the single-particle wave functions and eigenvalues of a noninteracting gas subject to the effective potential $v_s[\rho^M](r)$, Eq. (2b). Each f_{mj} denotes the occupation (0 or 1) of the jth orbital in the Slater determinant $|\phi_m\rangle$, where $|\phi_1\rangle,\ldots,|\phi_M\rangle$ are the lowest M noninteracting N-particle states corresponding to the single-particle equation (2a). The exchange-correlation potential $v_{xc}^M[\rho^M](r)$ is the functional derivative

$$v_{xc}^M[\rho^M](r)=\delta E_{xc}^M[\rho^M]/\delta\rho^M(r)\ , \tag{3}$$

the exchange-correlation energy functional $E_{xc}^M[\rho^M]$ being formally defined by

$$\begin{aligned}E_{xc}^M[\rho^M]=&\frac{1}{M}\sum_{m=1}^{M}\langle\psi_m\,|\,\hat{T}+\hat{U}\,|\,\psi_m\rangle\\&-\tfrac{1}{2}\int\int\frac{\rho^M(r)\rho^M(r')}{|r-r'|}d^3r\,d^3r'\\&-\frac{1}{M}\sum_{m=1}^{M}\langle\phi_m\,|\,\hat{T}\,|\,\phi_m\rangle\ .\end{aligned} \tag{4}$$

The $|\psi_m\rangle$ being of course unknown, an approximate scheme to determine $E_{xc}^M[\rho^M]$ is called for. On the basis of the local-density approximation for the thermal exchange-correlation energy functional $E_{xc}^\theta[\rho]$ and of the equivalence (valid for $M\to\infty$) between the canonical ensemble and the equiensemble, one such scheme has been recently derived.[5] Essential ingredients of this construction are (i) the equiensembles of N interacting and of N noninteracting electrons, both with multiplicity M and entropy $S=k\ln M$, where k is the Boltzmann constant, (ii) a canonical ensemble of N interacting electrons, with density $\rho(r)=\rho^M(r)$, at temperature θ chosen to make its entropy $S(\theta)$ equal to $k\ln M$, and (iii) a canonical ensemble of N noninteracting electrons, with density $\rho(r)=\rho^M(r)$, at temperature θ_s chosen to make its entropy $S_s(\theta_s)$ equal to $k\ln M$. Generally different, the two temperatures are approximately determined by the conditions

$$\int\sigma^\theta[\rho^M](r)d^3r=k\ln M \tag{5}$$

and

$$\int \sigma_s^{\theta_s}[\rho^M](r)d^3r = k \ln M \ . \tag{6}$$

Here and henceforth, for given r, the notation $f[\rho](r)$ indicates the quantity f (in this case σ^θ, the entropy per unit volume of an interacting gas at temperature θ, and $\sigma_s^{\theta_s}$, the entropy per unit volume of a noninteracting gas at temperature θ_s) calculated for a *homogeneous* system of density ρ equal to the local density $\rho(r)$. The assumed equivalence between the canonical ensemble and the equiensemble leads to the following approximation for the exchange-correlation energy functional:

$$E_{\rm xc}^M[\rho^M] \cong \int \{e_{\rm xc}^\theta[\rho^M](r) + t_s^\theta[\rho^M](r) - t_s^{\theta_s}[\rho^M](r)\} d^3r \ , \tag{7}$$

where $e_{\rm xc}^\theta$ is the exchange-correlation energy per unit volume of a homogeneous interacting gas and t_s^θ the kinetic energy per unit volume of a homogeneous noninteracting gas, both at temperature θ.

Combined with Eq. (7), Eq. (3) yields the exchange-correlation potential:

$$v_{\rm xc}^M[\rho^M](r) \cong \mu^\theta[\rho^M](r) - \mu_s^{\theta_s}[\rho^M](r) \ , \tag{8}$$

where μ^θ is the chemical potential of a homogeneous interacting gas at temperature θ, and $\mu_s^{\theta s}$ that of a homogeneous noninteracting gas at temperature θ_s.

To solve the self-consistent Eqs. (2) with the exchange-correlation potential in Eq. (8), we need expressions for the temperature-dependent functions of the density on the right-hand side of Eq. (7) and on the left-hand side of Eqs. (5) and (6). Approximate forms, taken from Refs. 8–11, are discussed in the Appendix.

Once the equiensemble density $\rho^M(r)$ is found, the following expression determines the equiensemble energy $\mathcal{E}(M)$, equal to the arithmetic average between the lowest M eigenvalues, $E_1, E_2, \ldots, E_M$, of H:

$$\mathcal{E}(M) = \frac{1}{M}\sum_{m=1}^{M}\sum_j f_{mj}\varepsilon_j - \frac{1}{2}\int\int \frac{\rho^M(r)\rho^M(r')}{|r-r'|}d^3r\,d^3r' - \int \rho^M(r) v_{\rm xc}^M(r) d^3r + E_{\rm xc}^M[\rho^M] \ . \tag{9}$$

From the $\mathcal{E}(M)$, the eigenvalues E_m can be easily computed. For degenerate spectra, we have shown in paper II that

$$\bar{E}_I = (M_I/g_I)[\mathcal{E}(M_I) - \mathcal{E}(M_{I-1})] + \mathcal{E}(M_{I-1}) \quad (I>1) \ , \tag{10}$$

where $\bar{E}_I$ and g_I denote the energy and the degeneracy of the Ith multiplet, respectively, and

$$M_I = \sum_{i=1}^{I} g_i \tag{11}$$

is the multiplicity of the ensemble constituted by the multiplets $i = 1, 2, \ldots, I$.

2. *Numerical procedure*

In order to calculate an excitation spectrum, its multiplet structure, i.e., the degeneracies of the levels and their relative order, must be known. Once the structure is found, e.g., by inspection of the experimental spectrum, the following sixfold procedure determines the excited energies.

(a) For a given multiplet, Eq. (11) determines $M = M_I$.

(b) The ground-state self-consistent density $\rho^{M=1}(r)$ provides an initial approximation for $\rho^{M=M_2}(r)$. For $I>2$, the self-consistent density $\rho^{M_{I-1}}(r)$ provides an initial approximation for $\rho^{M=M_I}(r)$. This approximation substituted for $\rho^M(r)$ in Eqs. (5) and (6), initial approximations for θ and θ_s are found.

(c) Substituted in Eq. (8), the approximate temperatures yield a functional form for the exchange-correlation potential. This form fixed, (i.e., θ and θ_s kept fixed), the self-consistent Eqs. (2) are solved iteratively, a step similar to the self-consistent solution of the ground-state Kohn-Sham equations.

(d) The resulting density substituted for $\rho^M(r)$ in Eq. (6), improved approximations θ' and θ_s' for the temperatures of the interacting and of the noninteracting systems are found.

(e) If θ' agrees with θ and θ_s' agrees with θ_s within, e.g., 0.1%, overall self-consistency has been achieved. If not, θ' and θ_s' are substituted for θ and θ_s, respectively, and steps (c)–(e) are repeated.

(f) Finally, the self-consistent density $\rho^M(r)$ and the self-consistent temperatures θ and θ_s are substituted in Eq. (7) to determine the exchange-correlation energy. The equiensemble energies, Eq. (9), can then be found and Eq. (10) determines the excited-state energies.

In concept, this sequence is only slightly more elaborate than the solution of the ground-state Kohn-Sham equations. Nonetheless, when applied to a Coulomb potential $v(r) = -Z/r$, it encompasses an inconspicuous difficulty requiring discussion. As pointed out in the introduction, this difficulty stems from assuming that, in the limit $M \to \infty$, the equiensemble becomes equivalent to the canonical ensemble. For a Coulomb potential, as for any potential with a continuous spectrum, the canonical ensemble is ill-defined, since the partition function diverges at any nonzero temperature. In practice, this results in logarithmically divergent exchange-correlation potentials in the limit of low densities, i.e.,

$$\lim_{\rho^M(r)\to 0} v_{\rm xc}^M[\rho^M](r) = \infty \ ,$$

so that step (c) cannot be executed.

To explain how this divergence arises, we refer to the expressions in the Appendix for the chemical potentials on the right-hand side of Eq. (8). In the classical regime, $\theta, \theta_s \gg \theta_F$, where $\theta_F = (3\pi^2\rho)^{2/3}/2k$ is the Fermi temperature, we have

$$\mu^\theta(\rho) \cong \mu_s^\theta(\rho) \cong \theta \ln\rho \ . \tag{12}$$

According to Eq. (8), then, at low densities

$$v_{\rm xc}^M[\rho^M](r) \cong (\theta - \theta_s)\ln\rho^M(r) \ . \tag{13}$$

Since, as shown in Sec. III, the interacting temperature θ exceeds the noninteracting temperature θ_s, the exchange-correlation potential becomes strongly attractive in the low-density tail of the charge distribution, creating a diffusive force that, in an infinite system, will drain all but an insignificant fraction of the charge away from the nucleus. In the canonical ensemble, this instability against ionization is readily understood, since at any finite temperature the thermal average encompasses ionized eigenstates of the atomic Hamiltonian. In the equiensemble, however, the effect is totally unphysical, because the average in Eq. (1) comprises only *bound* eigenstates.

To avoid this artifact of the assumed equivalence between the thermal ensemble and the equiensemble, we enclose the atomic system in a spherical box of radius R, i.e., we define the potential $v(r)$ in Eq. (2b) as

$$v(r)=\begin{cases}-Z/r & \text{for } r<R\\ \infty & \text{for } r\geq R.\end{cases}$$

By making their wave functions vanish at $r=R$, we ensure that both the interacting and the noninteracting systems have partition functions at all temperatures. The energies of the enclosed system will, naturally, depend on R; nevertheless, we find that, in the range 18 a.u. $\leq R \leq$ 140 a.u., the equiensemble energies vary typically by less than 0.1%, implying changes of less than 1% in the calculated binding energies. This indicates that, for R in this range, the differences between the eigenvalues of the confined and of the free Hamiltonian are negligible. Section III, which compares numerical results for the enclosed atom with experimental data for the free atom, dwells further on this point. Here, we consider another aspect of the self-consistent cycle.

Our choice of the multiplicities, Eq. (11), ensures that, averaged over full multiplets [see Eq. (1)], the equiensemble densities $\rho^M(r)$ be spherically symmetric. For the exact exchange-correlation potential, the solution of the Kohn-Sham equations must therefore make the right-hand side of Eq. (2c) spherically symmetric. For approximate forms of $v_{\rm xc}^M(\rho)$, however, a lopsided density may results from that equation, as the following discussion shows.

According to the definition of the occupation numbers f_{mi} on the right-hand side of Eq. (2c), the Kohn-Sham many-particle levels are filled in increasing energy order. If the ordering of the Kohn-Sham multiplets fails to match the ordering of the eigenvalues of the Hamiltonian, for some M the highest multiplet in the Kohn-Sham equiensembles will be partially filled. The Kohn-Sham Hamiltonian being an auxiliary entity devoid of physical meaning, such discrepancies between the interacting and noninteracting systems cannot be ruled out (even in the exact formalism). For an approximate exchange-correlation potential, they in principle constitute a problem, for a partially filled multiplet generally makes the right-hand side of Eq. (2c) asymmetric. In practice, however, one easily surmounts this difficulty by computing $\rho^M(r)$ as the *spherical average* of $\sum_{m=1}^{M}\sum_j f_{mj}\,|\,\varphi_j(r)\,|^2$. An example will be discussed in Sec. III.

B. The fractional occupation approach

1. Basic equations

Paper II, a generalization of the equiensemble formalism discussed in Sec. II A, develops a density-functional theory for unequally weighted ensemble densities. For given I ($I=1,2,\ldots$) and given w in the range $0\leq w\leq 1/M_I$, where M_I is determined by Eq. (11), the density is defined by

$$\rho_w^I(r)=\frac{1-wg_I}{M_{I-1}}\sum_{i=1}^{I-1}\sum_{k=1}^{g_i}\langle i,k\,|\,\hat{\rho}(r)\,|\,i,k\rangle + w\sum_{k=1}^{g_I}\langle I,k\,|\,\hat{\rho}(r)\,|\,I,k\rangle\ , \tag{14}$$

where $|\,i,k\,\rangle$ is the kth component of the g_i-degenerate ith multiplet in the spectrum of the interacting Hamiltonian $\hat{H}$.

To determine the $\rho_w^I(r)$ one must solve the self-consistent equations

$$-\tfrac{1}{2}\nabla^2\tilde{\varphi}_j(r)+\tilde{v}_s[\rho_w^I](r)\tilde{\varphi}_j(r)=\tilde{\varepsilon}_j\tilde{\varphi}_j(r)\ , \tag{15a}$$

$$\tilde{v}_s[\rho_w^I](r)=v(r)+\int\frac{\rho_w^I(r')}{|\,r-r'\,|}d^3r'+v_{\rm xc}^I[w;\rho_w^I](r)\ , \tag{15b}$$

and

$$\rho_w^I(r)=\frac{1-wg_I}{M_{I-1}}\sum_{m=1}^{M_I-g_I}\sum_j f_{mj}\,|\,\tilde{\varphi}_j(r)\,|^2 + w\sum_{m=M_I-g_I+1}^{M_I}\sum_j f_{mj}\,|\,\tilde{\varphi}_j(r)\,|^2\ , \tag{15c}$$

in a notation analogous to that of Eqs. (2). The exchange-correlation potential on the right-hand side of Eq. (15b) is the functional derivative

$$v_{\rm xc}^I[w;\rho](r)=\delta E_{\rm xc}^I[w;\rho]/\delta\rho(r)\ , \tag{16}$$

the exchange-correlation energy functional being formally defined by the relation

$$E_{\rm xc}^I[w;\rho_w^I]=\frac{1-wg_I}{M_{I-1}}\sum_{i=1}^{I-1}\sum_{k=1}^{g_i}\langle i,k\,|\,\hat{T}+\hat{U}\,|\,i,k\rangle+w\sum_{k=1}^{g_I}\langle I,k\,|\,\hat{T}+\hat{U}\,|\,I,k\rangle - \frac{1-wg_I}{M_{I-1}}\sum_{m=1}^{M_I-g_I}\langle\tilde{\phi}_m\,|\,\hat{T}\,|\,\tilde{\phi}_m\rangle-w\sum_{m=M_I-g_I+1}^{M_I}\langle\tilde{\phi}_m\,|\,\hat{T}\,|\,\tilde{\phi}_m\rangle-\tfrac{1}{2}\int\int\frac{\rho_w^I(r)\rho_w^I(r')}{|\,r-r'\,|}d^3r\,d^3r'\ . \tag{17}$$

The continuous variable w making this approach more flexible than the equiensemble formalism, two expressions ultimately relating the excitation energies of the interacting system, measured from the ground state energy,[12] to the single-particle eigenvalues of the noninteracting Hamiltonian were derived in paper II:

$$\bar{E}_I-\bar{E}_1=\frac{1}{g_I}\frac{d\mathcal{E}^I(w)}{dw}\bigg|_{w=w_I}+\sum_{i=2}^{I-1}\frac{1}{M_i}\frac{d\mathcal{E}^i(w)}{dw}\bigg|_{w=w_i}, \tag{18}$$

where w_i denotes an arbitrary real number in the interval $0\le w_i\le 1/M_i$, and the derivatives of the ensemble-averaged energies $\mathcal{E}^I(w)$ are given by

$$\frac{d\mathcal{E}^I(w)}{dw}=\sum_{j=N+M_{I-1}}^{N-1+M_I}\varepsilon_j-\frac{g_I}{M_{I-1}}\sum_{j=N}^{N-1+M_{I-1}}\varepsilon_j+\frac{\partial E^I_{\rm xc}[w;\rho]}{\partial w}\bigg|_{\rho=\rho^I_w}. \tag{19}$$

These expressions are exact, but for practical applications, an approximation for the partial derivative on the right-hand side of Eq. (19) is necessary. This constitutes the subject of Sec. II B 2.

2. *Approximate expressions for $v^I_{\rm xc}[w;\rho]$ and $\partial E^I_{\rm xc}[w;\rho]/\partial w$*

The quasi-local-density approximations for $E^M_{\rm xc}[\rho^M]$ and for $v^M_{\rm xc}$ derived in Ref. 5 apply only to equiensembles. For this reason, as discussed in paper II, our definition of the ensemble weights entering Eq. (14) was designed to interpolate between two sets of equiensemble weights: for given M_I, at $w=0$, the weights are all equal to $1/M_{I-1}$, corresponding to the equiensemble with multiplicity M_{I-1} and, at $w=1/M_I$, they are equal to $1/M_I$, corresponding to the equiensemble with multiplicity M_I. We now assume that the exchange-correlation energy functional and the exchange-correlation potential are smooth functions of the parameter w; from our definition of the ensemble weights, simple approximations for the exchange-correlation potential and for the partial derivative of the exchange-correlation energy with respect to the parameter w then follow. Specifically, we define $w_{1/2}=\frac{1}{2}M_I$ and expand $v^I_{\rm xc}[w;\rho^I_{w_{1/2}}]$ and $E^I_{\rm xc}[w;\rho^I_{w_{1/2}}]$ in Taylor series around $w=w_{1/2}$. We then find that

$$v^I_{\rm xc}[w_{1/2};\rho^I_{w_{1/2}}](r)=\tfrac{1}{2}\{v^{M_{I-1}}_{\rm xc}[\rho^I_{w_{1/2}}](r)+v^{M_I}_{\rm xc}[\rho^I_{w_{1/2}}](r)\}+O(1/M_I^2) \tag{20}$$

and

$$\frac{\partial E^I_{\rm xc}[w;\rho]}{\partial w}\bigg|_{\rho=\rho^I_{w_{1/2}}}=M_I\{E^{M_I}_{\rm xc}[\rho^I_{w_{1/2}}]-E^{M_{I-1}}_{\rm xc}[\rho^I_{w_{1/2}}]\}+O(1/M_I^3). \tag{21}$$

Notice that, as a result of the choice $w=w_{1/2}$, for large M_I the corrections on the right-hand sides are small. These corrections neglected, Eqs. (20) and (21) close the set of equations in Sec. II B 1, thus defining the procedure summarized in the following section.

3. *Numerical procedure*

Substituted in Eq. (20), the approximation (8) for the exchange-correlation potential associates four—and not two, as in the equiensemble density approach—temperatures $\theta(M_I)$, $\theta_s(M_I)$ [determined by substituting M_I for M in Eqs. (5) and (6), respectively], $\theta(M_{I-1})$, and $\theta_s(M_{I-1})$ [determined by substituting M_{I-1} for M in Eqs. (5) and (6), respectively] with the density $\rho^I_{w_{1/2}}$. Different, therefore, from the procedure in Sec. II A 2, the cycle solving Eqs. (15) deserves separate enumeration.

(a) Given I, Eq. (11) determines M_I and M_{I-1}.

(b) The ground-state self-consistent density gives an initial approximation for $\rho^{I=2}_{w_{1/2}}(r)$. Likewise, for $I>2$, the self-consistent solution for $\rho^{I-1}_{w_{1/2}}(r)$ provides an approximation for $\rho^I_{w_{1/2}}(r)$. As indicated above, Eqs. (5) and (6) then determine the initial approximations for $\theta(M_I)$, $\theta_s(M_I)$, $\theta(M_{I-1})$, and $\theta_s(M_{I-1})$.

(c) The approximate temperatures are substituted in Eq. (8), to provide approximations for $v^{M_I}_{\rm xc}[\rho^I_{w_{1/2}}](r)$ and for $v^{M_{I-1}}_{\rm xc}[\rho^I_{w_{1/2}}](r)$. Substituted in Eq. (20), these in turn provide an approximate functional form for the fractional occupation exchange-correlation potential. With this form fixed [i.e., with $\theta(M_I)$, $\theta_s(M_I)$, $\theta(M_{I-1})$, and $\theta_s(M_{I-1})$ fixed] the self-consistent Eqs. (15) are solved iteratively.

(d) Substituted in Eqs. (5) and (6), the resulting density yields improved approximations $\theta'(M_I)$, $\theta'_s(M_I)$, $\theta'(M_{I-1})$, and $\theta'_s(M_{I-1})$ for the four temperatures.

(e) If the four primed temperatures agree with the four unprimed ones [e.g., $\theta'(M_I)$ agrees with $\theta(M_I)$] within 0.1%, overall self-consistency has been achieved. If not, the new temperatures are substituted for the old ones [e.g., $\theta'(M_I)$ is subsituted for $\theta(M_I)$], and steps (c)–(e) are repeated.

(f) Finally, the self-consistent density $\rho^I_{w_{1/2}}(r)$ and the self-consistent temperatures $\theta(M_I)$ and $\theta_s(M_I)$ are substituted in Eq. (7) to determine $E^{M_I}_{\rm xc}[\rho^I_{w_{1/2}}]$. Likewise $\rho^I_{w_{1/2}}(r)$ and the self-consistent temperatures $\theta(M_{I-1})$ and $\theta_s(M_{I-1})$ are inserted in Eq. (7) to determine $E^{M_{I-1}}_{\rm xc}[\rho^I_{w_{1/2}}]$. Equation (21) then yields $\partial E^I_{\rm xc}[w;\rho]/\partial w\,|_{\rho=\rho^I_{w_{1/2}}}$, and the derivative $d\mathcal{E}^I(w)/dw$, needed to

compute the excitation energies in Eq. (18), is found from Eq. (19).

Since the potential in Eq. (20) derives from the quasi-local-density approximation in Ref. 5, the practical application of this cycle to a Coulomb potential runs into the difficulty mentioned in Sec. II A, associated with the logarithmic divergence of the exchange-correlation potential at low densities. To avoid this problem, again we must confine our atomic system. Already described in Sec. II A 2, this expedient will not be discussed here.

C. The transition-state approach

In Sec. III, we shall compare our numerical results with those of Slater's procedure.[7] This end in mind, we enumerate here the basic steps constituting that approach, referring the reader to Ref. 7 for a more comprehensive discussion of the approximations involved in the method. Basic to the procedure are self-consistent equations analogous to Eqs. (2) or (15):

$$-\tfrac{1}{2}\nabla^2\varphi_j^S(r)+v_s^S[\rho^S](r)\varphi_j^S(r)=\varepsilon_j^S\varphi_j^S(r)\ , \tag{22a}$$

$$v_s^S[\rho^S](r)=v(r)+\int\frac{\rho^S(r')}{|r-r'|}d^3r'+v_x[\rho^S](r)\ , \tag{22b}$$

and

$$\rho^S(r)=\left[\sum_{j=1}^{N}|\varphi_j^S(r)|^2+\sum_{j=1}^{\infty}f_j^S|\varphi_j^S(r)|^2\right]\Big/2\ , \tag{22c}$$

where $v_x[\rho]$ denotes the ground-state exchange potential, and f_j^S is the occupation (0 or 1) of the orbital j in the excited state being considered. The occupation of the orbital $\varphi_j^S(r)$ lies therefore halfway between the occupations of the jth orbitals in the ground state and in the excited state.

Once Eqs. (22) are solved, the following approximate expression relates the excited-state energy E^S to the single-particle eigenvalues ε_j^S:

$$E^S-E_1=\sum_{j=1}^{\infty}f_j^S\varepsilon_j^S-\sum_{j=1}^{N}\varepsilon_j^S\ , \tag{23}$$

thus determining the excitation energy reckoned from the ground-state energy E_1.

The ground-state potential on the right-hand side of Eq. (22b) greatly simplifies the solution of the self-consistent equations: in contrast with Eqs. (2) and (5)–(8), or (15)–(16), Eqs. (22) involve no temperature, hence bypassing steps (d) and (e) in the cycles discussed in Sec. II A 2 and II B 3. Moreover, the ground-state exchange potential vanishes in the limit of low densities, so that the atomic system need not be confined.

The procedure is thus convenient for practical applications. As illustrated by our numerical results, it is also reasonably accurate. Nevertheless, in spite of these attractive qualifications, Eqs. (22) and (23), derived[7] by applying the ground state Hartree-Fock-Slater formalism[7,13] to excited states, lack the logical foundation underlying the formalism in Secs. II A and II B. A discussion of those equations in the framework of density-functional theory is therefore instructive, and we shall next show that, for a highly degenerate first excited state, they follow from a simple approximation in the fractional occupation approach.

We consider the ensemble constituted by the ground state and the first excited multiplet of the Hamiltonian $\hat{H}$. We assume that the ground state is nondegenerate and that the first excited state has degeneracy g. The ensemble multiplicity is then $M=1+g$. For $w=w_{1/2}=\frac{1}{2}M$, Eq. (15c) becomes

$$\rho_w^{I=2}(r)=\frac{1+g/2}{1+g}\sum_{j=1}^{N}|\tilde{\varphi}_j(r)|^2+\frac{1/2}{1+g}\sum_{m=2}^{g+1}\sum_j f_{mj}|\tilde{\varphi}_j(r)|^2\ .$$

Furthermore, since

$$f_{mj}=\begin{cases}1, & 1\le j\le N-1\\ \delta_{j,(N-1+m)}, & j\ge N\end{cases}$$

we find

$$\rho_w^{I=2}(r)=\frac{1+g/2}{1+g}\sum_{j=1}^{N}|\tilde{\varphi}_j(r)|^2+\frac{g/2}{1+g}\left[\sum_{j=1}^{N-1}|\tilde{\varphi}_j(r)|^2+\frac{1}{g}\sum_{m=2}^{g+1}|\tilde{\varphi}_{N-1+m}(r)|^2\right]\ . \tag{24}$$

In the limit $g\to\infty$, this equation becomes equivalent to Eq. (22c) (provided an average over the multiplet is introduced in Slater's method; in practice, this is in fact an indispensable complement of the transition-state approach, necessary to preserve the symmetry of the exchange potential). If the ground-state exchange potential $v_x[\rho](r)$ is substituted for $v_{xc}^{I=2}[w;\rho](r)$, the entire set of Eqs. (15) becomes equivalent to Eqs. (22). Likewise, if the ground-state exchange energy functional is substituted for $E_{xc}^{I=2}[w;\rho]$, so that $\partial E_{xc}^{I=2}[w;\rho]/\partial w=0$, Eq. (18), combined with Eq. (19), yields $\bar{E}_2-\bar{E}_1=\varepsilon_{N+1}-\varepsilon_N$, equivalent to Eq. (23).

For a highly degenerate first excited state, therefore, the approximation $E_{xc}^{I=2}[w;\rho]=\int e_x[\rho](r)d^3r$, where $e_x[\rho]$ denotes the ground-state exchange energy per unit volume of a homogeneous system with density ρ, reduces the fractional occupation approach to the transition-state approach. Since excited states are often highly degenerate, since the exchange-correlation potentials for the ground state and for the lowest excited multiplets should be approximately equal, since correlation energies are normally much smaller than the exchange energies, and since the derivative $\partial E_{xc}^{I=2}[w;\rho]/\partial w$ is generally small—a point discussed in Sec. III—Slater's method should generally yield accurate first excitation energies. This is in line with our numerical results for the fourfold degenerate first excited state of He. In this case, $\partial E_{xc}^{I=2}[w;\rho]/\partial w$ amounting to less than 2% of $\bar{E}_2-\bar{E}_1$, the excitation energy derived from Eq. (23) is only 5% larger than the experimental value.

This argument provides an alternative derivation of the transition-state formulas, one that is firmly grounded on the exact developments in paper II. If generally valid, it would provide a means to improve systematically Slater's prescription. Correlation and more accurate descriptions of the exchange-correlation potential would be easily appended to the method. Unfortunately, however, our reasoning applies only to highly degenerate first excited states; it cannot be extended to $I>2$. For, since the ensemble average on the right-hand side of Eq. (15c) involves all eigenstates with $i=1,2,\ldots,I$, while the right-hand side of Eq. (22c) involves only $i=1$ and $i=I$, the densities $\rho_w^{I>2}(r)$ and $\rho^S(r)$ are irreconcilably different. In general, as pointed out in the Introduction, the transition state approach is not a special case of, but an alternative to the formulation described in Sec. II B 1.

III. NUMERICAL RESULTS

A. Spectra

The very small spin-orbit splittings in the excitation spectrum[6,14] of He are often neglected,[6] so that the eigenstates are classified as *para* (spin-0) or *ortho* (spin-1) states. In a cruder approximation, in this work we disregard the splittings associated with the electronic spin and consider only the average between the para and ortho energies corresponding to each state, with weights one and three, respectively. Depicted as binding energies, i.e., subtracted from the ionization threshold $E_1^{+\text{expt}}=-1.807$ Ry, the lowest ten such averages are displayed as bold solid lines in Fig. 1. In a one-particle picture, each of these eigenstates comprises one electron in the hydrogenic $1s$ state and the other electron in a hydrogenic nl state. This defines the labeling system in the figure, each level being labeled by the principal quantum number n and the total angular momentum $L\equiv l$.

Also depicted in Fig. 1 are the lowest ten excited levels, calculated by the equiensemble density and the fractional occupation approach, represented by the solid and the dashed lines, respectively. In the equiensemble method, Eq. (10) yields the eigenvalues of $\hat{H}$. To determine the binding energies E_I^b displayed in the figure, we had to calculate the ground-state energy E_1^+ of He^+. To this end, we considered the $1s$ orbital with occupation $f_{1s}^{m=1}=1$, solved Eqs. (2) for $M=1$, and inserted the resulting density in Eq. (9). This gave $E_1^+=-3.725$ Ry. The binding energies were then easily obtained: $E_I^b=\bar{E}_I-E_1^+$.

In the fractional occupation approach, in contrast, Eq. (18) determines the excitation energies measured from a reference multiplet[12] I_0. In Fig. 1, we chose the highest depicted multiplet, $I=11$, as reference; the binding energies were therefore computed as $E_I^b=\bar{E}_I-\bar{E}_{11}+E_{11}^b$ the last term denoting the experimental binding energy of the eleventh multiplet: $E_{11}^b=-0.045$ Ry.

The two calculated spectra are in excellent mutual agreement: each excitation energy in the fractional density approach differs by less than 1% from the corresponding energy in the equiensemble density approach. This shows that, as expected, neglecting the terms of $O(1/M_I^2)$ and $O(1/M_I^3)$ on the right-hand sides of Eqs. (20) and (21), respectively, constitutes a satisfactory approximation. The two methods produce comparably accurate results.

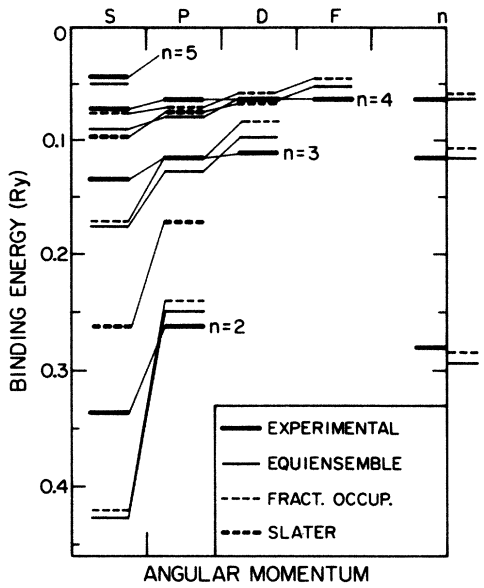

FIG. 1. Energies computed in the equiensemble density (solid lines), fractional occupation (dashed lines), and transition state (bold dashed lines) approaches, compared with the ten lowest excited levels in the experimental spectrum of He (bold solid lines). Averaged over spin, classified by total electronic angular momentum, the levels associated with the same principal quantum number n, defined in the text, are joined. As explained in the text, all energies are reckoned from the ionization threshold. The transition-state energies are shown only for $n=2$ and 3, to avoid overcrowding. On the right vertical axis, the equiensemble density and the fractional occupation energies averaged over spin and angular momentum are compared with the averaged experimental energies.

Inferior, yet still satisfactory, is the agreement between the numerical and the experimental spectra. The calculated binding energies are typically 20% off the measured binding energies. The deviations follow a pattern. For the smallest angular momenta associated with each principal quantum number n, the binding energies are overestimated; for the largest angular momenta, they are underestimated. We nevertheless observe that remarkably accurate results are obtained for the average energies of the almost degenerate states corresponding to $n=2,3,4,\ldots$. To show this, for each n the right-hand vertical axis in Fig. 1 compares $E_n^b=\sum_{L=0}^{n-1}[(2L+1)E_{nL}^b]/n^2$, the averages over angular momentum and spin of the energies computed in the equiensemble density and in the fractional occupation approaches, with the corresponding experimental average. In all cases, the agreement is excellent.

With hindsight, we might rationalize this finding by three qualitative considerations. Formally speaking, all deviations in the equiensemble density approach (and a large component of the deviations in the fractional density approach) are due to errors in the equiensemble exchange-correlation energy functional, $E_{xc}^M[\rho(r)]$. (1)

These errors, $\delta E_{xc}^{M}[\rho(r)]$, will include fluctuations with M, for every increment $M \rightarrow M+1$. The *fractional* significance of these fluctuations is then decreased when average energies for a group of states between M and $M+\Delta M(\Delta M>1)$ are calculated. (2) The approximate equivalence of equi- and thermal ensembles is poorly satisfied when energy differences between two successive levels are small compared to $k\theta$ (or $k\theta_s$). One therefore expects a good representation only for such values of M that nearly degenerate multiplets are either totally included or totally omitted. (3) Since we make a local-density approximation, we expect best results for those equiensembles whose electronic structure best resembles that of a uniform thermal ensemble. We suggest that all these considerations may, in different degrees, help explain the numerically observed accuracy of the average energies for each value of the principal quantum number.

Even when the significantly less accurate angular-momentum-resolved energies are considered, the density functional results for the excitation spectrum compare favorably with the results of Slater's transition-state prescription. In Fig. 1, the latter are shown as bold dashed lines, obtained by subtracting the difference E^S-E_1, Eq. (23), from the experimental ionization energy $\Delta E \equiv E_1^+ - E_1 = 1.807$ Ry. In contrast with the slanted pattern displayed by the other two computed spectra in Fig. 1, the bold dashed lines lie systematically above the bold solid lines. The average deviation of the calculated energies from the experimental values is approximately 40%, a figure comparable to the *largest* deviations (i.e., the deviations found in the computation of the nS levels), but considerably larger than the *average* deviations in the equiensemble density and the fractional occupation approaches. Generally speaking, therefore, the methods in Secs. II A and II B constitute improvements over the transition-state approach.

The two highest energies in Fig. 1 constitute the only example found in this work of mismatch between the interacting and the noninteracting eigenvalues, a possibility discussed in general terms at the end of Sec. II A 2. In solving the self-consistent Eqs. (2), we have found that the $5S$ noninteracting level lies below the $4F$ noninteracting level, in disagreement with the experimentally determined ordering of the interacting energies. Thus, while the interacting $I=10$ equiensemble comprises the $1S$, $2S$, $2P$, $3S$, $3P$, $3D$, $4S$, $4P$, $4D$, and $4F$ multiplets, the noninteracting $I=10$ equiensemble comprises the $1S$, $2S$, $2P$, $3S$, $3P$, $3D$, $4S$, $4P$, $4D$, and $5S$ multiplets and 24 components of the $4F$ multiplet. Both ensembles have 117 levels, but the partially filled $4F$ multiplet in the Kohn-Sham ensemble makes their symmetries different. As prescribed in Sec. II A 2, to avoid an asymmetrical density we have averaged the right-hand side of Eq. (2c) over all angular orientations of the vector $\mathbf{r}$ and have otherwise followed the cycle (a)–(e) to compute the equiensemble energy $\mathcal{E}(117)$, needed to determine both the $4F$ and the $5S$ eigenvalues [see Eq. (18)]. All other noninteracting equiensembles comprise only full multiplets, no spherical averaging being necessary.

Table I collects other data extracted from our numeri-

TABLE I. Equiensemble energies $\mathcal{E}(M_I)$ $(I=1,2,\ldots,11)$, computed in the equiensemble density approach, and differences between equiensemble energies $\Delta\mathcal{E}(M_I)=\mathcal{E}(M_I)-\mathcal{E}(M_{I-1})$ $(I=2,3,\ldots,11)$, computed in the fractional occupation approach, compared with the corresponding experimental values. All energies are in rydbergs. For comparison, below each computed energy the exchange-only approximation to the same quantity is shown within parentheses. For each ensemble, the multiplicity M_I and the highest multiplet are also listed.

I	State	M_I	$\mathcal{E}(M_I)$	$\mathcal{E}^{\text{expt}}(M_I)$	$\Delta\mathcal{E}(M_I)$	$\Delta\mathcal{E}^{\text{expt}}(M_I)$
1	$1S$	1	−5.672	−5.807		
			(−5.447)			
2	$2S$	5	−4.452	−4.630	1.2398	1.1770
			(−4.256)		(1.1896)	
3	$2P$	17	−4.111	−4.370	0.3458	0.2601
			(−3.919)		(0.3380)	
4	$3S$	21	−4.070	−4.325	0.0406	0.0450
			(−3.896)		(0.0313)	
5	$3P$	33	−3.990	−4.249	0.0829	0.0765
			(−3.832)		(0.0649)	
6	$3D$	53	−3.925	−4.197	0.0670	0.0518
			(−3.772)		(0.0597)	
7	$4S$	57	−3.917	−4.188	0.0082	0.0088
			(−3.765)		(0.0075)	
8	$4P$	69	−3.896	−4.166	0.0200	0.0215
			(−3.747)		(0.0181)	
9	$4D$	89	−3.871	−4.143	0.0243	0.0233
			(−3.726)		(0.0209)	
10	$4F$	117	−3.848	−4.124	0.0231	0.0193
			(−3.706)		(0.0198)	
11	$5S$	121	−3.845	−4.121	0.0025	0.0026
			(−3.704)		(0.0022)	

cal calculations. Of special interest are the equiensemble energies and the differences between equiensemble energies, computed in the equiensemble density and the fractional occupation approaches, respectively. The equiensemble energies are all larger than the equiensemble averages of the experimental energies, also shown in the table. Since this applies, in particular, to the ground-state energy, $E_1 \equiv \mathcal{E}(M=1)$, it is instructive to recall a few conclusions drawn from studies of the ground state.[15,16]

The ground-state energies of He and He^+ have been calculated in both the local-density approximation[15] (LDA) and the local-spin-density approximation[16] (LSDA) for the exchange-correlation energy functional. The computed energies lie above the experimental values. More recently,[17] it has been recognized that, to a large extent, these discrepancies are due to the self-interactions in the classical Coulomb energy

$$U_c = \tfrac{1}{2}\int\int \frac{\rho(r)\rho(r')}{|r-r'|} d^3r\, d^3r' .$$

As Eq. (4) suggests, in an exact formulation, symmetric terms in the exchange-correlation energy functional would cancel out these spurious interactions. In the LDA and in the LSDA, however, the self-interactions are only partially canceled by the approximate exchange-correlation functional; this makes the ground-state energies too large. In particular, for the singlet ground state of He, the two approximations are identical, yielding[18] $E_1^{\mathrm{LDA}} \equiv E_1^{\mathrm{LSDA}} = -5.67$ Ry $> E_1^{\mathrm{expt}} = -5.81$ Ry. For the spin-degenerate He^+ ground state, on the other hand, the results of the LDA and of the LSDA are substantially different. The cancellation of the self-interactions being much more complete in the latter than in the former, the LSDA estimate[16] ($E_1^{+\mathrm{LSDA}} = -3.92$ Ry) is much closer to the experimental energy ($E_1^{+\mathrm{expt}} = -4.00$ Ry) than the LDA estimate[18] ($E_1^{+\mathrm{LDA}} = -3.72$ Ry).

Consider now the equiensemble energies for $M_I > 1$. While in the ground state two electrons with opposite spin share the $1s$ orbital, in the excited state they need not have opposite spins and they occupy different orbitals. This suggests that, for $M_I > 1$, a spin-polarized generalization of the methods in Secs. II A and II B is necessary to compute accurately the $\mathcal{E}(M_I)$. By ignoring spin, our treatment is bound to produce relatively large errors. In particular, for large M_I we expect it to yield equiensemble energies approaching $E_1^{+\mathrm{LDA}}$, the LDA estimate for the He^+ ground state, and not $E_1^{+\mathrm{LSDA}}$. This is ratified by Table I.

In light of our discussion of the ground state, we expect that, even if a spin-density calculation were carried out, the residual self-interactions would make the equiensemble energies significantly larger than the experimental averages. As in the ground-state calculations, we expect that, contributing approximately equally to the atom and to the ion, these residual interactions partially cancel each other and become relatively unimportant in the binding energies.

At present, unfortunately, neither a spin-density generalization of the quasi-local-density approximation of Ref. 5 nor accurate expressions for the thermodynamical functions of a spin-polarized homogeneous electron gas are available, so that no spin-density analogue of Table I can be constructed. To compensate for this shortcoming, we have subtracted the excited state energies from $E_1^{+\mathrm{LDA}}$ (and not from $E_1^{+\mathrm{LSDA}}$, as we would have done in a spin-density calculation) to produce the binding energies in Fig. 1. The self-interactions in the ionized state canceling those in the excited states, this procedure improves substantially the numerical results; nonetheless, it may be a poor substitute for the spin-density approach. In particular, inspection of the experimental spectrum shows that, while the para configuration of the nS states is nearly degenerate with the other nL ($L > 1$) levels, the ortho configuration has considerably lower energy. In a spin-density formalism, therefore, one should be able to resolve the splitting between the para and the ortho nS levels, which would considerably improve Fig. 1.

Table I also shows that the differences $\Delta\mathcal{E}(M_I)$ between successive equiensemble energies, computed in the fractional occupation approach, are on the average within 20% of the $\Delta\mathcal{E}(M_I)$ calculated from experimental excitation energies. The absolute deviations from the experimental values thus diminish as M_I grows. The derivation[5] of Eq. (7), which assumes that the equiensembles and thermal ensembles are equivalent, an assumption justified only for large M, explains this trend of the numerical results and suggests that, to minimize the error in computing the excitation energies, one measure them from the highest energy considered in the computation, i.e., from $E_{I=11}$. This is what we have done in Fig. 1.

Equiensemble energies and differences between equiensemble energies, computed in the exchange-only approximation to the exchange-correlation energy functional are shown within parentheses in Table I. Although the $\mathcal{E}(M_I)$ calculated in this fashion deviate considerably more from the experimental equiensemble energies than the $\mathcal{E}(M_I)$ calculated with correlation, the ground-state energy for He^+ in the exchange-only approximation ($E_1^+ = -3.61$ Ry) is also farther from the experimental energy than the E_1^+ calculated with correlation. As a result, *reckoned from the ionization threshold,* the equiensemble energies computed in the exchange-only and in the exchange-correlation approximations are rather similar. This is also true of the differences between equiensemble energies computed in the fractional occupation approach, Table I showing that, although correlation brings most of the differences closer to the experimental values, especially for small M_I some of the $\Delta\mathcal{E}(M_I)$ computed in the exchange-only approximation agree better with the corresponding $\Delta\mathcal{E}^{\mathrm{expt}}(M_I)$. Correlation nevertheless affects dramatically the accuracy of our results for the energies averaged over angular momentum. As the notches on the right vertical axis of Fig. 1 show, all energies computed in the exchange-correlation approximation are within a few percent of the experimental energies. In contrast, deviations around 30% result in the exchange-only approximation. The correlation contributions to the excitation energies are therefore very important.

As explained in Secs. II A 2 and II B 3, the solution of the Kohn-Sham equations in both the equiensemble density and the fractional occupation approach yields self-consistent temperatures, determined by Eqs. (5) and (6).

TABLE II. The self-consistent temperatures θ and θ_s, computed in the equiensemble density approach, and the self-consistent temperatures $\theta(M_I)$, $\theta_s(M_I)$, $\theta(M_{I-1})$, and $\theta_s(M_{I-1})$, computed in the fractional occupation approach, for $I=2,3,\ldots,11$. All temperatures are in units of $(10^{-2}$ Ry$)/k$, where k is the Boltzmann constant.

I	θ	θ_s	$\theta(M_I)$	$\theta_s(M_I)$	$\theta(M_{I-1})$	$\theta_s(M_{I-1})$
2	2.51	2.64	3.33	2.94	0	0
3	4.98	4.34	6.63	5.67	1.67	2.04
4	3.09	2.97	4.12	3.75	3.34	3.18
5	2.13	2.02	2.95	2.79	1.87	1.94
6	1.85	1.64	2.24	2.05	1.53	1.43
7	1.80	1.58	1.88	1.65	1.78	1.57
8	1.60	1.36	1.82	1.58	1.60	1.38
9	1.38	1.14	1.60	1.36	1.36	1.13
10	1.26	1.03	1.43	1.19	1.20	0.98
11	1.25	1.02	1.25	1.04	1.24	1.02

The temperatures found in the runs listed in Table I are displayed in Table II. Similar trends are observed in the two approaches. In particular, the interacting temperatures generally exceed the noninteracting temperatures, so that, as pointed out in Sec. II A 2, the exchange-correlation potential diverges in the limit of low densities. All temperatures being nevertheless small ($k\theta \approx 20$ mRy), the equiensemble energies of the confined atomic system depend weakly on the radius R of the enclosing box.

To show this, for four I (1, 3, 6, and 10) and for various radii ranging from 18 to 140 a.u., Table III lists the equiensemble energies $\mathcal{E}(M_I)$, computed in the equiensemble density approach. The energies are generally insensitive to changes in the box radius. As expected, the energies associated with the lowest, more localized states are much less sensitive than those associated with the higher excitations. To compute the energy of the $I=6$ (i.e., $3D$) state, for instance, $R=35$ a.u. would have been adequate. Conversely, to compute eigenvalues with $I>11$, $R>70$ a.u. would be necessary. As a general rule, for each I, a broad range of radii can be found in which the self-consistent cycles of Secs. II A and II B converge to energies very weakly dependent on R. Thus, provided that the radius be appropriately chosen, one can guarantee that the confinement of the atomic system distort the excitation energies by no more than 1%. On the basis of this criterion, all energies in Table I were computed with $R=70$ a.u.

B. Effective potentials and densities

This section presents illustrative potentials and densities found by solving the self-consistent Eqs. (2). Since the fractional occupation approach yields qualitatively similar results, we here restrict ourselves to discussing the equiensemble density method.

Plotted in Fig. 2 as functions of the radial distance r, the effective equiensemble potentials, Eq. (2b), for $I=6$ and 10, are compared with the ground-state potential ($I=1$). For $r\to 0$, all three curves approach the nuclear potential $v(r)=-2/r$. At large radial distances, however, the two higher equiensemble potentials depart markedly from the ground-state potential and, for increasing r in the range 60 a.u. $<r\leq R=70$ a.u., they become progressively more attractive.

This behavior, stemming from the logarithmic dependence of the exchange-correlation potential on the density [cf. Eq. (13)], has been discussed in Sec. II A. Here, we note that in this low-density region, the small tempera-

TABLE III. Equiensemble energies $\mathcal{E}(M_I)$ for $I=1$, 3, 6, and 10, and various radii R of the spherical box confining the He atom. All energies are in rydbergs.

R (a.u.)	$\mathcal{E}(1)$	$\mathcal{E}(3)$	$\mathcal{E}(6)$	$\mathcal{E}(10)$
17.5	−5.678	−4.112	−3.912	−3.794
35.0	−5.678	−4.112	−3.924	−3.844
70.0	−5.678	−4.112	−3.925	−3.847
140.0	−5.678			−3.849

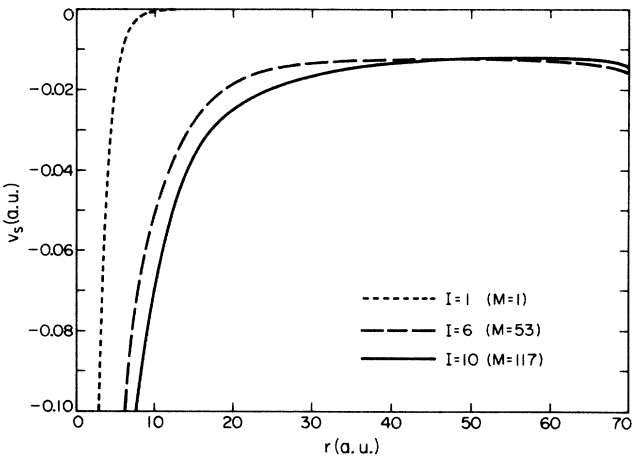

FIG. 2. Effective equiensemble potentials [Eq. (2b)] for the ground state ($I=1$) and the sixth and tenth equiensembles as functions of the radial distance r in the range $0\leq r\leq R$, where $R=70$ a.u. denotes the radius of the spherical box enclosing the atom. In all cases, for small r, the Coulomb potential $v(r)=-2/r$ is dominant. In the opposite extreme, $r\cong R$, the minute density makes the ground-state potential nearly zero; by contrast, as Eq. (13) shows, for increasing r the effective potentials for $I>1$ become progressively more attractive.

tures in Table II make the potential relatively weak, even for $r \approx R$. This fortunate circumstance allowed us to work with the relatively large box radii in Table III. We note, however, that as R increases, the convergence of the cycles described in Secs. II A 2 and II B 3 is progressively slowed: magnified box radii make the potential more negative near $r=R$, hence drain more charge away from the nucleus and make the temperatures θ and θ_s, given by Eqs. (5) and (6), more sensitive to the charge distribution near $r=R$—all effects reducing the stability of the self-consistent cycles. The computational cost, as well as the accuracy of the calculation, must therefore be weighed in specifying the radius.

Figure 3 displays the radial equiensemble densities $4\pi r^2 \rho^{M_I}(r)$ ($I=1$, 6, and 10) as functions of r. The curves are strongly peaked at $r \cong 0.5$ a.u.; the area under this peak is the occupation of the very localized $1s$ orbital, equal to two in the ground state and larger than unity in all cases. The broader, less distinct maxima in the plots for $I>1$ correspond to the occupied n shells: $n=2$ and 3 for $I=6$ and $n=2$, 3, and 4 for $I=10$. Near the box wall, as a result of the attractive potentials in Fig. 2, the equiensemble densities for $I=6$ and 10 are enormously larger than the ground-state density. Still, in atomic units they are small, $\rho^{M_6} \cong \rho^{M_{10}} \approx 10^{-7}$. Because of these reduced densities, and of the moderate effective potential, the region $r \cong R$ contributes little to the equiensemble energies; for this reason, the equiensemble energies depend weakly on R, as our discussion of Table III pointed out.

From the equiensemble densities, the densities ρ_I associated with the excited states are easily calculated. From Eq. (1) we find

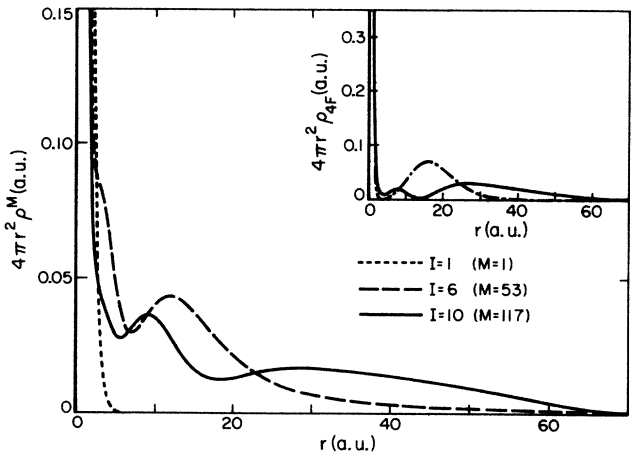

FIG. 3. Radial densities for the ground state, and for the sixth and tenth equiensembles as functions of the radial distance. As discussed in the text, the peaks in each plot correspond to the principal quantum number n entering the equiensemble; e.g., corresponding to $n=1$, 2, 3, and 4, the $I=10$ curve has a strong maximum at $r<1$ a.u., followed by a shoulder, a peak at $r \cong 10$ a.u., and a broader maximum around $r=30$ a.u., respectively. The inset shows that Eq. (25) (solid line) reproduces poorly the expected density for the $4F$ state, Eq. (26) (dashed-dotted line).

$$\rho_I(r)=[M_I \rho^{M_I}(r)-M_{I-1}\rho^{M_{I-1}}(r)]/g_I \ . \tag{25}$$

The inset in Fig. 3 depicts the average radial density $4\pi r^2 \rho_{4F}$, associated with the $4F$ ($I=10$) multiplet. Given the large angular momentum of this highly excited state, the density should be accurately described by the one-electron picture introduced in Sec. III A, i.e., by the expression

$$4\pi r^2 \rho_{4F}(r)=r^2[\,|R^2_{1s}(r)|^2+|R^1_{4f}|^2\,] \ , \tag{26}$$

where R^Z_{nl} denotes the radial part of the hydrogenic wave function for atomic number Z, principal quantum number n, and angular momentum l. This radial density, plotted as a dashed-dotted line in the inset, disagrees strikingly with the density obtained from Eq. (25). Especially, the dashed-dotted line displays a maximum at $r=16$ a.u., contrasting markedly with the two maxima in the solid plot. This discrepancy, reflecting errors [greatly enhanced by the subtraction on the right-hand side of Eq. (25)] in the computation of the equiensemble densities, reiterates the conclusion extracted from Fig. 1, that our attempt to resolve the splitting between nearly degenerate states [in this case the $4D$ ($I=9$) and the $4F$ ($I=10$) multiplets] exceeds the limitations of the approximate Eqs. (7) and (8).

IV. CONCLUSIONS

In this work two numerical procedures based on a density-functional formalism for excited states were applied to the He atom. One of the procedures is the equiensemble density method, introduced formally by Theophilou[4] and made practical by the quasi-local-density approximation,[5] Eq. (7), for the equiensemble exchange-correlation energy functional. The other procedure is the fractional occupation method, derived in paper II; for practical purposes, it relies on the approximations suggested by Eqs. (20) and (21), again founded on Eq. (7). Applied to a highly degenerate first excited multiplet this second approach is a refinement of the transition-state approach;[7] in general, however, Slater's prescription and the fractional occupation method are irreconcilable.

For each principal quantum number $n=2$, 3, and 4 in the one-particle excitation spectrum, the numerical results of both procedures agree very well with the mean energies obtained by averaging the experimental binding energies over angular momentum and spin. The splittings between states with the same n but different angular momenta are nevertheless grossly overestimated, showing that the density-functional methods described in Sec. II are unable to resolve small energy differences.

This inference has annoying implications. It means that the methods in Secs. II A and II B will generally produce blurred pictures of the experimental spectra. It also means that semiquantitative knowledge of the splittings in the experimental spectrum is required before an accurate calculation can be carried out. Consequently, only existing experimental spectra can be reproduced; unknown spectra cannot be predicted.

These considerations apply to accurate computa-

tions—at the 1% level—of the binding energies. If deviations of the order of 20% are acceptable, the finer structure of the experimental data will be poorly reproduced, but the density-functional methods will determine the spectrum, provided only that the ordering of the levels be known or guessed. As Fig. 1 further indicates, the resulting energies will generally be significantly more accurate than those predicted by a transition-state calculation. Thus, even if the approximations in Eqs. (7) and (8) are stretched to their limits, the equiensemble density and the fractional occupation methods will yield satisfactorily accurate results.

Finally, we emphasize that this first density-functional calculation of an excitation spectrum admits refinements. Most evidently, a spin-density generalization of Eqs. (2), or of Eqs. (15), is called for. Here, the traditional extension[16] underlying the local spin-density approximation for the ground-state exchange-correlation energy functional is unfortunately inadequate: lacking rotational invariance, it would for instance artificially separate the $S_z=0$ component of each ortho configuration from its $S_z=\pm 1$ components. Accounting for spin remains therefore an open problem.

The simple form of Eqs. (18) and (19) suggests a second, more exciting line of research. Eq. (21), a simple-minded interpolation based on the quasi-local-density approximation for the exchange-correlation energy functional, brought the fractional occupation approach into alignment with the equiensemble density approach. Alternative forms for $\partial E_{\rm xc}^{M}[w;\rho]/\partial w$, derived independently of the quasi-local-density approximation, can improve the fractional occupation formulation beyond the equiensemble density method, to overcome the limitations exposed in Fig. 1. We hope that our study will stimulate work in this direction.

ACKNOWLEDGMENTS

This work was supported by the National Science Foundation under Grant No. DMR-87-03434. Partial support for one of us (E.K.U.G.) from the Deutsche Forschungsgemeinschaft (West Germany) and for another (L.N.O.) from the Conselho Nacional de Desenvolvimento Científico e Tecnológico (Brazil) is gratefully acknowledged.

APPENDIX A

Equations (5) and (6), determining the temperatures θ and θ_s, and Eqs. (7) and (8), determining the equiensemble exchange-correlation energy functional and potential, respectively, involve various thermodynamical functions for the homogeneous interacting and noninteracting electron gases. This appendix describes the computation of the necessary quantities. Specifically, we are interested in the following functions.

(i) For the homogeneous noninteracting gas (density ρ and temperature θ_s): the chemical potential $\mu_s^{\theta_s}(\rho)$, required in Eq. (8), the kinetic energy per unit volume $t_s^{\theta_s}(\rho)$, required in Eq. (7), and the entropy per unit volume $\sigma_s^{\theta_s}(\rho)$, entering Eq. (6).

(ii) For the homogeneous interacting gas (density ρ, temperature θ): the exchange-correlation chemical potential $\mu_{\rm xc}^{\theta}(\rho)$, the exchange-correlation energy per unit volume $e_{\rm xc}^{\theta}(\rho)$, and the exchange-correlation entropy per unit volume $\sigma_{\rm xc}^{\theta}(\rho)$. Note that $e_{\rm xc}^{\theta}$ enters Eq. (7), while, added to the noninteracting functions $\mu_s^{\theta}(\rho)$ and $\sigma_s^{\theta}(\rho)$, the functions $\mu_{\rm xc}^{\theta}(\rho)$ and $\sigma_{\rm xc}^{\theta}(\rho)$ yield the interacting chemical potential $\mu^{\theta}(\rho)$ and the entropy per unit volume $\sigma^{\theta}(\rho)$ in Eqs. (8) and (5), respectively.

1. Noninteracting gas

Accurate expressions for $\mu_s^{\theta_s}(\rho)$ (Ref. 8) and $t_s^{\theta_s}(\rho)$ (Ref. 11) are available. The free energy per unit volume in a homogeneous noninteracting gas, on the other hand, is[11]

$$f_s^{\theta_s}(\rho)=\mu_s^{\theta_s}(\rho)\rho-\tfrac{2}{3}t_s^{\theta_s}\ , \tag{27}$$

so that the entropy per unit volume is

$$\sigma_s^{\theta_s}(\rho)=[\tfrac{5}{3}t_s^{\theta_s}(\rho)-\mu_s^{\theta_s}(\rho)\rho]/\theta_s\ . \tag{28}$$

2. Exchange

Reference 11 presents an excellent parametrization for the exchange contribution to the chemical potential, $\mu_x^{\theta}(\rho)$. In order to compute the exchange contribution to the interacting-gas energy per unit volume, given by

$$e_x(\rho)=\tfrac{3}{2}\mu_0^{x}(\rho)\rho-f_x^{\theta}(\rho)\ , \tag{29}$$

we need the exchange contribution to the free energy per unit volume, f_x^{θ}. To this end, noting that $\lim_{\rho\to 0}f_x^{\theta}(\rho)=0$, we write

$$f_x^{\theta}(\rho)=\int_0^{\rho}\mu_x^{\theta}(\rho')d\rho'\ , \tag{30}$$

and compute the right-hand side by numerical integration. Given the superior accuracy of the parametrization[11] for $\mu_x^{\theta}(\rho)$, the free energy thus obtained comes closer to the numerical results for $f_x^{\theta}(\rho)$ in Ref. 9 than the parametrized f_x^{θ} in Ref. 9. Moreover, unlike the latter parametrization, in the low-temperature regime, $\theta\ll\theta_F$, Eq. (30) correctly produces the weak logarithmic singularity[11] $f_x^{\theta}(\rho)-f_x^{0}(\rho)\approx-\theta^2\ln\theta$.

Once f_x^{θ} is obtained, e_x^{θ} [Eq. (29)], and the exchange contribution to the entropy, given by

$$\sigma_x^{\theta}=[\tfrac{3}{2}\mu_x^{\theta}(\rho)\rho-2f_x^{\theta}]/\theta\ , \tag{31}$$

are easily determined.

3. Correlation

Reference 11 reviews recent efforts to calculate the correlation contribution to the thermodynamical functions of a homogeneous electron gas. At zero temperature, excellent parametrizations $\hat{\mu}_c(\rho)$ and $\hat{e}_c(\rho)$ for the correlation chemical potential and the correlation energy per unit volume are available.[19] At nonzero temperatures, unfortunately, no comparably reliable expressions exist. Uncertainties of up to 5% are estimated for the

most accurate parametrization[10] $\tilde{f}_c^{\theta}(\rho)$ for the free energy per unit volume. To compute the correlation contributions to the chemical potential and to the entropy per unit volume, we have to differentiate numerically this parametrization, a procedure that magnifies the uncertainties in the free energy:

$$\tilde{\mu}_{xc}^{\theta}(\rho)=\left[\frac{\partial \tilde{f}_{xc}^{\theta}(\rho)}{\partial \rho}\right]_{\theta} \tag{32}$$

and

$$\tilde{\sigma}_{xc}^{\theta}(\rho)=-\left[\frac{\partial \tilde{f}_{xc}^{\theta}(\rho)}{\partial \theta}\right]_{\rho} . \tag{33}$$

The uncertainties in $\tilde{f}_c^{\theta}(\rho)$ and $\tilde{\sigma}_{xc}^{\theta}(\rho)$ are further enhanced in the exchange-correlation energy per unit volume, obtained from

$$\tilde{e}_{xc}^{\theta}(\rho)=\tilde{f}_{xc}^{\theta}(\rho)+\theta\tilde{\sigma}_{xc}(\rho) . \tag{34}$$

At temperatures small compared with the Fermi temperature, the parametrization $\tilde{f}_{xc}^{\theta}(\rho)$ becomes particularly inaccurate.[10] To ensure that our approximations for the correlation contributions to the chemical potential and to the exchange-correlation energy per unit volume be accurate at low temperatures, we subtract from Eqs. (32) and (34) the zero-temperature values of $\tilde{\mu}_{xc}^{\theta}(\rho)$ and of $\tilde{e}_{xc}^{\theta}(\rho)$, and add to them the more accurate zero-temperature expressions of Ref. 19, i.e., we determine the excess chemical potential and the exchange-correlation energy per unit volume from

$$\mu_{xc}^{\theta}(\rho)=\mu_x^{\theta=0}(\rho)+\hat{\mu}_c(\rho)+[\tilde{\mu}_{xc}^{\theta}(\rho)-\tilde{\mu}_{xc}^{\theta=0}(\rho)] , \tag{35}$$

and

$$e_{xc}^{\theta}(\rho)=e_x^{\theta=0}(\rho)+\hat{e}_c(\rho)+[\tilde{e}_{xc}^{\theta}(\rho)-\tilde{e}_{xc}^{\theta=0}(\rho)] , \tag{36}$$

where $\mu_x^{\theta}(\rho)$ and $e_x^{\theta}(\rho)$ denote the exchange contributions to the chemical potential and the exchange-correlation energy per unit volume, respectively.

Similarly, we calculate the excess entropy from

$$\sigma_{xc}^{\theta}(\rho)=\tilde{\sigma}_{xc}^{\theta}(\rho)-\tilde{\sigma}_{xc}^{\theta=0}(\rho) . \tag{37}$$

For temperatures comparable to or larger than the Fermi temperature, these manipulations introduce large uncertainties in $\mu_{xc}^{\theta}(\rho)$, $e_{xc}^{\theta}(\rho)$, and $\sigma_{xc}^{\theta}(\rho)$. Fortunately, the correlation contributions amount to typically 10% of the energies in Table I. Moreover, the largest part of those contributions comes from high-density regions, where the Fermi temperature is small compared to θ, so that Eqs. (35)–(37) are accurate. Thus, even errors as large as 20% in these equations will produce small deviations—a few percent, at most—in the calculated binding energies.

*Permanent address: Instituto de Física e Química de São Carlos, Universidade de São Paulo, 13 560 São Carlos, São Paulo, Brazil.

[1]E. K. U. Gross, L. N. Oliveira, and W. Kohn, paper I, Phys. Rev. A **37**, 2805 (1988).

[2]E. K. U. Gross, L. N. Oliveira, and W. Kohn, paper II, Phys. Rev. A **37**, 2809 (1988).

[3]A. K. Theophilou, J. Phys. C **12**, 5419 (1979).

[4]For a review of ground-state density-functional theory, see, e.g., W. Kohn and P. Vashishta, in *Theory of the Inhomogeneous Electron Gas,* edited by S. Lundqvist and N. H. March (Plenum, New York, 1983), p. 79.

[5]W. Kohn, Phys. Rev. A **34**, 737 (1986).

[6]H. Bethe and E. Salpeter, *Quantum Mechanics of One- and Two-Electron Atoms* (Springer-Verlag, Berlin, 1957).

[7]J. C. Slater, *The Self-Consisted Field for Molecules and Solids: Quantum Theory of Molecules and Solids* (McGraw-Hill, New York, 1974), Vol. IV, p. 51.

[8]M. W. C. Dharma-wardana and R. Taylor, J. Phys. C **14**, 629 (1981).

[9]F. Perrot and M. W. C. Dharma-wardana, Phys. Rev. A **30**, 2619 (1984).

[10]S. Tanaka, S. Mitake, and S. Ichimaru, Phys. Rev. A **32**, 1896 (1985).

[11]R. G. Dandrea, N. W. Ashcroft, and A. E. Carlsson, Phys. Rev. B **34**, 2097 (1986).

[12]To simplify the comparison with the Slater formula (see Sec. II C), we reckon the excitation energies from the ground state. Equation (18) can nevertheless be trivially generalized to yield the energy $\bar{E}_I$ measured from an arbitrary multiplet I_0. Taking advantage of this flexibility, in Sec. III A we shall present the fractional occupation energies reckoned from the $5S$ state (i.e., from $I_0=11$).

[13]J. C. Slater, Phys. Rev. **81**, 385 (1951).

[14]W. C. Martin, J. Phys. Chem. Ref. Data **2**, 257 (1973).

[15]B. Y. Tong and L. J. Sham, Phys. Rev. **144**, 1 (1966).

[16]O. Gunnarsson and B. I. Lundqvist, Phys. Rev. B **13**, 4274 (1976).

[17]J. P. Perdew and A. Zunger, Phys. Rev. B **23**, 5048 (1981).

[18]The calculated ground-state energies, dependent on the approximation for the exchange-correlation energy functional, vary from author to author. For definiteness, we list here the LDA energies obtained in our computations, based on the parametrized form proposed in Ref. 19, and the LSDA energy for He^+ quoted in Ref. 16.

[19]S. H. Vosko, L. Wilk, and M. Nusair, Can. J. Phys. **58**, 1200 (1980).